Supporting Information for

A ferromagnetically coupled, bell-shaped [Ni$_4$Gd$_5$] cage

Foteini E. Kakaroni,[‡] Demetrios I. Tzimopoulos,[†] Hector W. L. Fraser,[§] Milosz Siczek,[ʃ] Tadeusz Lis,[ʃ] Marco Evangelisti,*[#] Euan K. Brechin*[§] and Constantinos J. Milios*[‡]

[‡]*Department of Chemistry, The University of Crete, Voutes, 71003, Herakleion, Greece. E-mail:* komil@uoc.gr

[†]*Department of Chemistry, Aristotle University of Thessaloniki, 54124 Thessaloniki, Greece.*

[§]*EaStCHEM School of Chemistry, The University of Edinburgh, David Brewster Road, Edinburgh, EH9 3FJ, UK. E-mail:* ebrechin@staffmail.ed.ac.uk

[ʃ]*Department of Chemistry, University of Wroclaw, 50-283 Wroclaw, Poland.*

[#]*Instituto de Ciencia de Materiales de Aragón (ICMA), CSIC – Universidad de Zaragoza, 50009 Zaragoza, Spain. E-mail:* evange@unizar.es
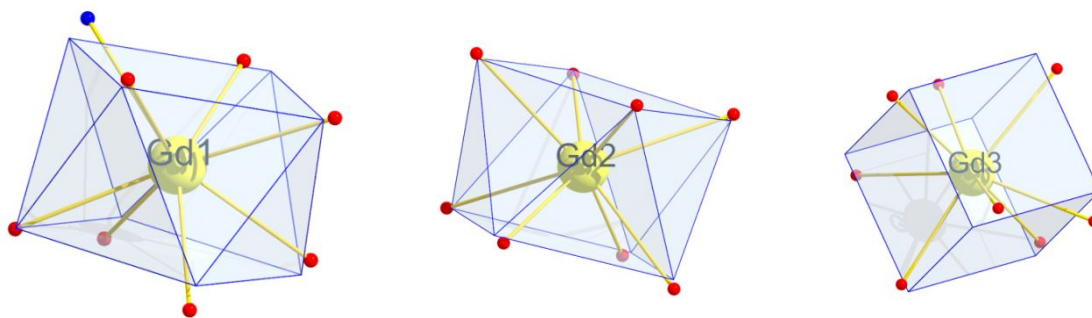
Fig. S1. The coordination geometries of the Gd(III) metal centers in **1**: Gd1 - Square antiprism; Gd2 - Square antiprism; Gd3 - Cube.
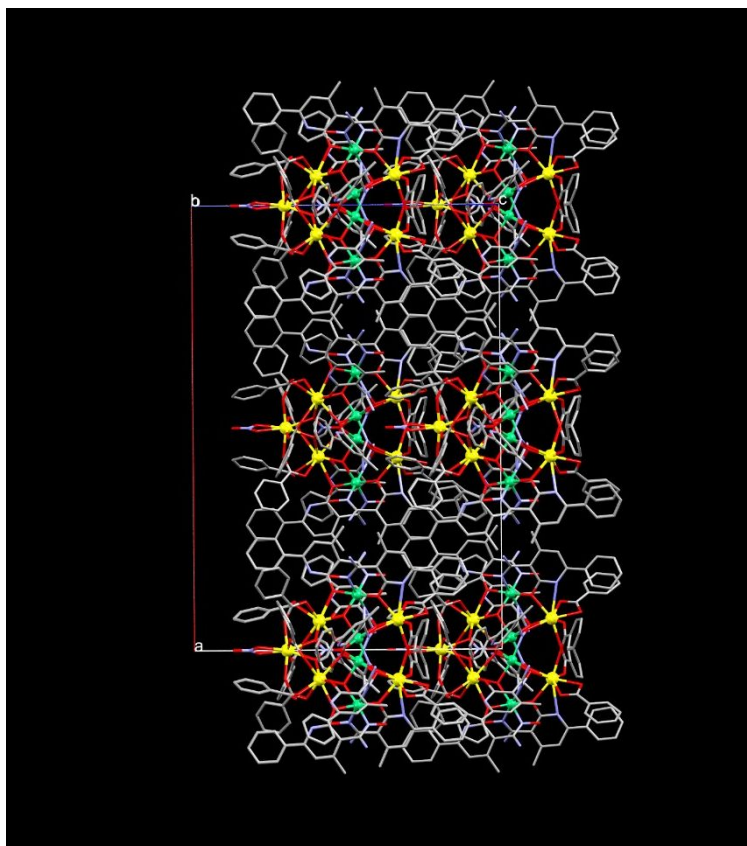

Fig. S2. View of the crystal packing of **1** down the *b* axis. H-atoms and solvate molecules have been omitted for clarity.

Table S1. Continuous Shape Measures Calculation for Structure [ML8].

	OP-8	HPY-8	HBPY-8	CU-8	SAPR-8	TDD-8	JGBF-8	JETBPY-8	JBTPR-8
Gd1	4.173	19.610	16.128	12.163	2.759	3.411	33.060	16.215	27.614
Gd2	28.958	23.341	16.728	10.148	0.475	2.176	15.350	27.291	1.757
Gd3	31.176	24.440	6.350	6.003	7.028	6.659	7.167	22.539	6.379

OP-8:Octagon; HPY-8: Heptagonal pyramid; HBPY-8: Hexagonal bipyramid; CU-8: Cube; SAPR-8: Square antiprism; TDD-8: Triangular dodecahedron ; JGBF-8: Johnson gyrobifastigium J26; JETBPY-8: Johnson elongated triangular bipyramid J14; JBTPR-8: Biaugmented trigonal prism J50.

SHAPE is a program for the stereochemical analysis of molecular fragments and geometries. It calculates continuous shape measures of a set of points (e.g. atomic positions) relative to the vertices of ideal polygons or polyhedral, either centered or non-centered. In addition, it also calculates deviations from minimal distortion paths and polyhedral interconversion generalized coordinates. For more information see the following references:

(a) Pinsky M.; Avnir D. Continuous Symmetry Measures. 5. The Classical Polyhedra. *Inorg. Chem.* **1998**, *37,* 5575-5582.
(b) Casanova D.; Cirera J.; Llunell M.; Alemany P.; Avnir D.; Alvarez S. Minimal Distortion Pathways in Polyhedral Rearrangements*. J. Am. Chem. Soc.* **2004**, *126*, 1755-1763.
(c) Cirera J.; Ruiz E.; Alvarez S. Shape and Spin State in Four-Coordinate Transition-Metal Complexes: The Case of the d[6] Configuration. *Chem. Eur. J.* **2006**, *12*, 3162 – 3167.

X-ray diffraction. At first, a crystal of **1** was mounted on the diffractometer at 100 K under a cold nitrogen gas stream supplied by an Oxford Cryostream. However, preliminary data collection showed multi-twinning and crystal cracking. Therefore a new crystal was coated in perfluoropolyalkylether oil (1800 cSt) and mounted on a thin quartz fiber attached to a copper pin at room temperature and slowly cooled to 230 K. Data collection were performed at this temperature. Upon father cooling to 80 K the crystal cracked and data obtained at this temperature were not suitable for publication. The same procedure was applied to complex **2**; in this case crystal did not crack and it was possible to obtain diffraction data at 100 K.
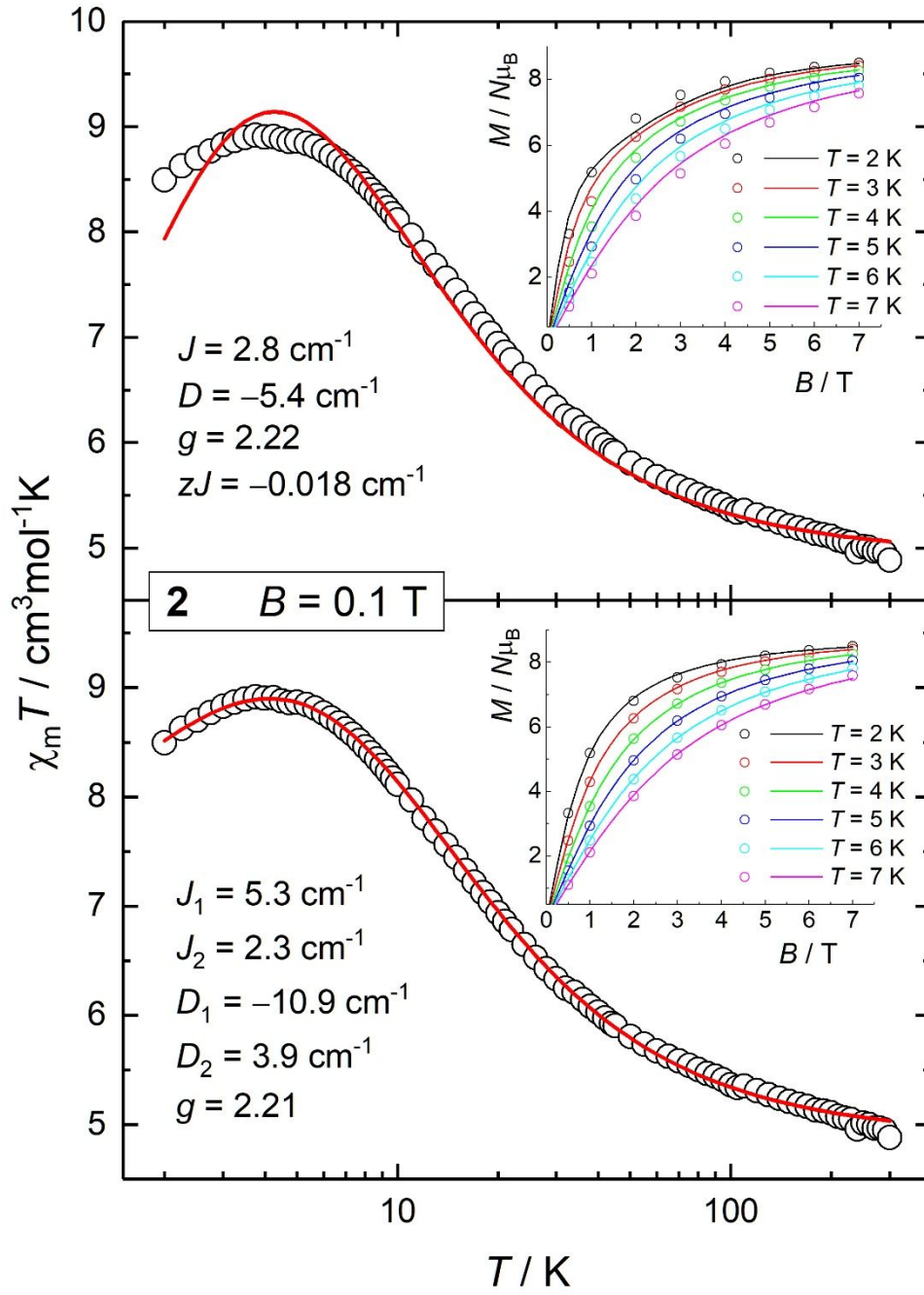
Fig. S3. Comparison between fit results (solid lines) of the susceptibility and magnetization data (insets) of **2** for the "1-J + 1-D" model (top) and the "2-J + 2-D" model (bottom), respectively. Note that, when adopting the "1-J + 1-D" model, the intermolecular interaction term zJ' is needed to account for the $\chi_m T$ decrease at the lowest temperatures.
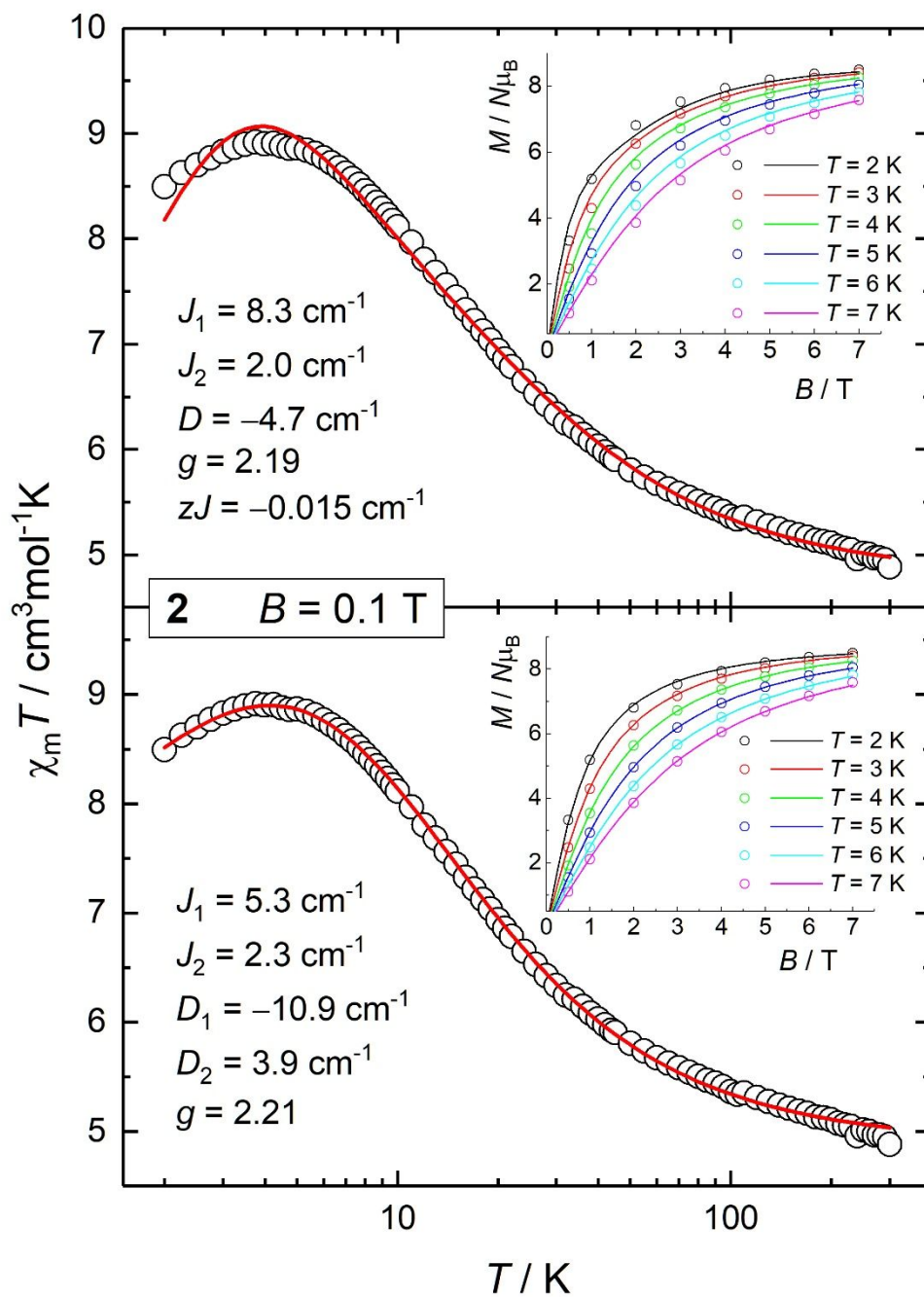
Fig. S4. Comparison between fit results (solid lines) of the susceptibility and magnetization data (insets) of **2** for the "2-*J* + 1-*D*" model (top) and the "2-*J* + 2-*D*" model (bottom), respectively. Note that, when adopting the "2-*J* + 1-*D*" model, the intermolecular interaction term *zJ′* is needed to account for the $\chi_m T$ decrease at the lowest temperatures.
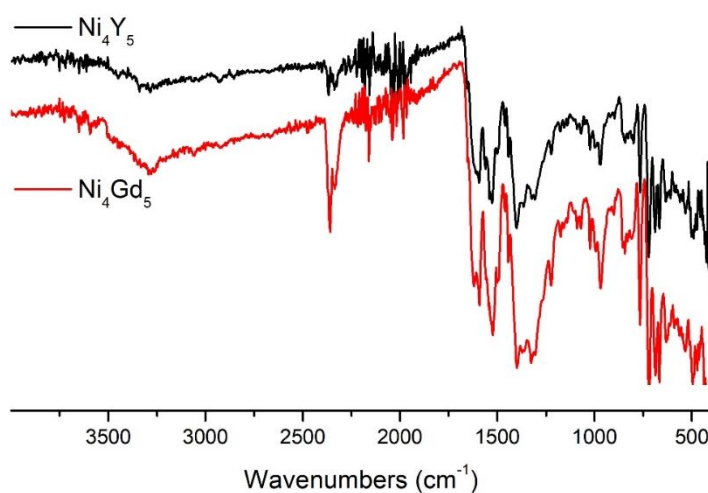
Fig. S5. FTIR-ATR spectra of **1** and **2** in the 4000-440 cm^{-1} range (on a microcrystalline sample).
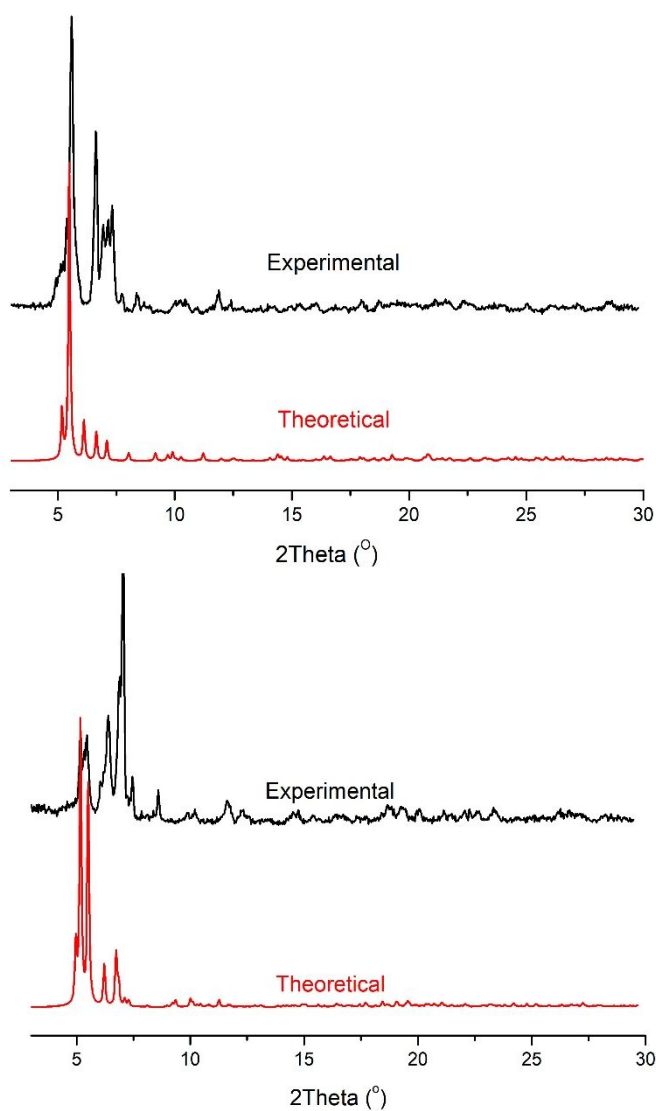

Fig. S6. Powder XRD (Cu source) diagrams' comparison between the experimental and theoretical patterns for complexes **1** (top) and **2** (bottom) in the 3-30° 2θ range. The difference

in the peaks' intensity is probably due to partial decomposition of the crystals caused by loosing of solvate molecules.

Table S2. Crystallographic data for complexes **1** and **2**.

	1·13.6MeCN·H_2O	**2**·3H_2O
Formula[a]	$C_{201.2}H_{189.8}ClGd_5N_{39.6}Ni_4O_{44.5}$	$C_{174}H_{155}Cl_{0.5}N_{26.5}Ni_4O_{49}Y_5$
M_W	4931.06	4098.35
Crystal System	orthorhombic	orthorhombic
Space group	Aba2	Pca2$_1$
a/Å	34.062(18)	33.774(8)
b/Å	28.836(8)	26.005(7)
c/Å	23.494(7)	22.958(6)
V/Å^3	23076(13)	20164(9)
Z	4	4
T/K	230	100
λ^b/Å	0.71073	0.71073
D_c/g cm^{-3}	1.419	1.350
μ(Mo-Ka)/ mm^{-1}	1.82	1.87
Meas./indep.(R_{int}) refl.	30634/16426 (0.053)	76800/33809 (0.104)
Obs. refl. [$I>2\sigma(I)$]	13220	11993
$wR2^{c,d}$	0.218	0.420
Data/parameters/restraints	16426/1267/136	33809/1930/674
$R1^{d,e}$	0.077	0.122
Goodness of fit on F^2	1.08	1.03
$\Delta\rho_{max,min}$/ eÅ^{-3}	2.20, −2.64	1.02, -0.48

^{a} Including solvate molecules Mo-Kα radiation, graphite monochromator. ^{c} $wR2= [\Sigma w(|F_o^2|-|F_c^2|)^2/ \Sigma w|F_o^2|^2]^{1/2}$. ^{d}For observed data. ^{e} $R1= \Sigma||F_o|- |F_c||/ \Sigma|F_o|$.